


# Quantum dynamics of positron-hydrogen scattering and three-body bound state formation with an assisting laser field: predictions of a reduced-dimensionality model

Xiao Hu Ji<sup>1,2</sup>, Li Guang Jiao<sup>1,3,4,\*</sup> , Aihua Liu<sup>2,\*</sup> , Yong Zhi Zhang<sup>5</sup>, Uwe Thumm<sup>6,\*</sup>  and Yew Kam Ho<sup>7</sup> 

<sup>1</sup> College of Physics, Jilin University, Changchun 130012, People's Republic of China

<sup>2</sup> Institute of Atomic and Molecular Physics, Jilin University, Changchun 130012, People's Republic of China

<sup>3</sup> Helmholtz-Institut Jena D-07743 Jena, Germany

<sup>4</sup> GSI Helmholtzzentrum für Schwerionenforschung GmbH, D-64291 Darmstadt, Germany

<sup>5</sup> College of Physical Science and Technology, Heilongjiang University, Harbin 150080, People's Republic of China

<sup>6</sup> James R. Macdonald Laboratory, Department of Physics, Kansas State University, Manhattan, KS 66506-2604, United States of America

<sup>7</sup> Institute of Atomic and Molecular Sciences, Academia Sinica, Taipei 10617, People's Republic of China

E-mail: [lgjiao@jlu.edu.cn](mailto:lgjiao@jlu.edu.cn), [aihualiu@jlu.edu.cn](mailto:aihualiu@jlu.edu.cn) and [thumm@phys.ksu.edu](mailto:thumm@phys.ksu.edu)

Received 5 August 2023, revised 19 November 2023

Accepted for publication 10 January 2024

Published 25 January 2024



## Abstract

We investigate the quantum dynamics of target excitation and positronium formation in the positron-hydrogen atom scattering without and with an external assisting laser field within a reduced-dimensional quantum model. Strong interference fringes between the incident and reflected positron wave packets are observed in the reaction region. We further investigate the critical behavior of transition probabilities near the channel-opening thresholds for hydrogen excitation and positronium formation and find a strong competition between channels with similar threshold energies, but different parities. The transmission ratios of the incident positron in different reaction channels are calculated, and it is shown that only positronium formation in the ground state prefers forward scattering. Our simulation of the positron-hydrogen scattering with an assisting laser field indicates that the three-particle bound states can be formed during the collisions due to the photon emission induced by the external laser field.

Supplementary material for this article is available [online](#)

Keywords: positron–hydrogen scattering, positronium formation, reduced quantum model, time-dependent Schrödinger equation

\* Authors to whom any correspondence should be addressed.

## 1. Introduction

Positron scattering from atoms has been continuously attracting considerable interest in both theoretical and experimental investigations of matter-antimatter interactions since the discovery of positrons [1–4]. Compared to electron-atom scattering, positronium (Ps) formation and positron-electron annihilation complicates the positron scattering problem tremendously and causes a formidable challenge to theoretical modeling of the collision dynamics [4]. In the past decades, great progress has been made on both experimental measurement and theoretical prediction of the cross sections for positron-atom scattering [3–6]. For simple atomic targets, such as hydrogen and helium, the cross sections in various reaction channels have been benchmarked in the literature [7, 8]. Recent interest in positron physics has been focused on, for example, positron scattering with atoms and molecules [6, 9], resonances in positron-atom systems [10, 11], positron attachment and annihilation in molecules and condensed matter [12, 13], and positron scattering in plasma environments [14, 15] and in static electromagnetic fields or ultrashort intense laser fields [16–18].

Theoretical approaches to positron-atom scattering can be generally divided into two categories, time-independent and time-dependent methods. The former group employs formal scattering theory and focuses primarily on the scattering amplitudes from initial to final states, in most cases without explicitly calculating the total scattering wave function. Methods devoted to low-energy scattering are, e.g. the Kohn and Schwinger variational methods [19]. Intermediate-energy scattering (from the opening of the first inelastic channel to dozens of eV above the ionization threshold) involves the complicated couplings between different reaction channels. The close-coupling with pseudostates [20], coupled-channel optical potential [21], hyperspherical close-coupling [22], and the convergent close-coupling [23] methods have been established to tackle the complexities of the collision dynamics in this energy region. For high-energy scattering (far above the ionization threshold), perturbative approaches, e.g. the second-order Born [24], distorted-wave Born [25], continuum distorted-wave [26], and polarized orbital [27] methods can be applied reasonably well to capture the asymptotic behavior of the scattering wave function. So far these time-independent methods have produced accurate scattering amplitudes, phase shifts, and cross sections in the elastic, excitation, ionization, and Ps formation channels, for a variety of atoms and in a wide range of impact energies [3, 4].

Time-dependent methods, in addition to scattering amplitudes and cross sections, provide dynamic information about the reaction process and spatio-temporal evolution of the system wave function in more detail. Similar to the standard close-coupling methods, the time-dependent close-coupling (TDCC) method has been developed to follow the dynamic time-evolution of the system and extract scattering amplitudes from the final system wave function [28]. To our knowledge, the first successful application of the TDCC method to positron-hydrogen collisions was performed by Plante and

Pindzola [29], where good agreement with experimental measurements and time-independent theoretical calculations was obtained. The later TDCC works of Yamanaka and Kino [30, 31] have explicitly extracted Ps formation and direct positron annihilation cross sections in positron-hydrogen collisions. Time-dependent classical trajectory Monte Carlo (CTMC) calculations with suitably chosen initial conditions for the incident positron and target atom, allow investigations of the dynamics of the scattering system by tracing the trajectories of both electron and positron. To name a few, this method has been successfully employed by Naginey *et al* [14, 32] to estimate the positronium formation cross sections for positron scattering from hydrogen-like ions, and by Pandey *et al* [15] to investigate the positronium formation of positron-alkali-metal atoms scattering in Debye plasmas. Recently, Liu *et al* [18] have developed a CTMC approach with Heisenberg (CTMC-H) potentials [33], which enabled the extension of classical-trajectory simulations to the low-energy regime. Their results are in good agreement with quantum-mechanical calculations, even at energies near the ionization threshold [34].

In this work, we investigate positron-hydrogen atom scattering by directly solving the time-dependent Schrödinger equation (TDSE) on a spatio-temporal numerical grid [35]. In full dimensionality, even for the simplest positron-hydrogen system, one generally needs to discretize one time dimension and six space dimensions (three for the positron and the other three for the electron). Performing the time evolution of the system wave function in complete six-dimensional space is still a formidable task, even on today's supercomputers [36–38]. In the present work, we adopt a one-dimensional scattering model that has been extensively applied to laser-assisted scattering [39–43]. Although the motion of the positron and electron is restricted along a straight line, our reduced-dimensionality numerical modeling provides a good balance between computational ease and retention of characteristic features of the quantum-mechanical three-body system, such as correlation and channel-opening and -closing effects.

Another aspect that motivates the present work stems from the currently growing interest in laser-assisted ion-, electron-, and positron-atom scattering [44–50]. With the fast development of laser technologies, intense laser fields have become a powerful tool to control and manipulate scattering processes. It is worth noting that laser-assisted electron scattering has been experimentally investigated by several groups [51–53]. Laser-assisted positron scattering might be feasible in the near future. From a theoretical point of view, when the scattering system is exposed to an intense laser pulse, the traditional perturbation treatment of the laser interaction in the framework of time-independent scattering theory fails [54–56]. In this case, one generally needs to solve the TDSE non-perturbatively and trace the modulation effect of the laser field on the time-resolved scattering amplitudes. Recently, Liu *et al*. [18, 33] employed the CTMC-H method and showed that intense laser fields can significantly modulate the ionization cross sections in electron-hydrogen scattering [33] and the Ps formation in positron-hydrogen scattering [18]. To this end, it

is of great interest to perform a non-perturbative full quantum-mechanical investigation on these scattering processes and take a detailed survey on the spatio-temporal resolution of the scattering dynamics. Keeping in mind that the numerical TDSE method has achieved great success in modeling the non-linear dynamics of atomic and molecular systems in intense laser fields [35, 57], as well as the fact that a strong laser field directs the motion of charged particles in the polarization direction [58], the reduced-dimensionality TDSE investigation of the scattering system provides an alternative and powerful tool for interpreting the novel phenomena observed in numerically expensive full-dimensionality quantum-mechanical calculations. More interestingly, our simulation shows that the formation of stable positron-hydrogen-bound states is possible during and after the collision, assisted by a laser field. This finding may open up a novel approach for controlling and manipulating the formation of positronic-bound states.

This paper is organized as follows. In section 2, we introduce our one-dimensional model for positron–hydrogen atom scattering and numerical method for solving the TDSE. Detailed discussion of the scattering dynamics is provided in section 3, including interference fringes in positron density distributions, the critical behavior of transition probabilities near the channel-opening thresholds, the variation of populations and transmission ratios with respect to the incident energy, and the formation of positron–hydrogen bound states in the laser-assisted collision. We summarize our work in section 4. Atomic units are used throughout this work unless otherwise specified.

## 2. Theoretical method

Since the hydrogen atom is much heavier than the electron and positron, we assume that the nucleus remains fixed at the origin of our coordinate system ( $x$ -axis) during the scattering. The Hamiltonian of the system in one dimension is given by [39–43]

$$H = \frac{1}{2}p_1^2 + \frac{1}{2}p_2^2 + V(x_1) - V(x_2) - V(x_1 - x_2), \quad (1)$$

where  $p_1$  ( $p_2$ ) and  $x_1$  ( $x_2$ ) are, respectively, the momentum and coordinate of the positron (electron). We use the soft-core Coulomb potential [59]

$$V(x) = \frac{1}{\sqrt{x^2 + a^2}}, \quad (2)$$

to represent the effective interaction between charged particles in the one-dimensional model. The merit of the soft-core Coulomb potential has been well established in a variety of investigations on laser-atom interactions and laser-assisted ion-atom scattering [35, 45, 48, 58]. In the present work, we follow the choice of Larkin *et al.* [39] by setting  $a = 1$ , so that a quantitative comparison to the previous work can be made.

The eigenenergies of the H and Ps atoms are obtained by directly solving the time-independent two-body Schrödinger equation with the finite-difference technique. Our numerical

calculations of the bound-state energies are in good agreement with the prediction of Larkin *et al* [39] in all reported digits. The energy differences between the initial ground state of the H atom and bound states of H and Ps atoms determine the channel-opening threshold energies  $E_{th}$ . In this work, we are interested in the lowest several inelastic channels, for which

$$E_{th} = \begin{cases} 0.08164\dots & p + \text{Ps}(1) \\ 0.39488\dots & e^+ + \text{H}(2) \\ 0.49121\dots & p + \text{Ps}(2) \\ 0.51833\dots & e^+ + \text{H}(3) \\ 0.57680\dots & p + \text{Ps}(3) \\ 0.57712\dots & e^+ + \text{H}(4) \\ \dots & \dots \\ 0.66982\dots & \text{ionization} \end{cases}. \quad (3)$$

Here, the integer  $n$  in  $\text{H}(n)$  and  $\text{Ps}(n)$  represents the quantum number of the one-dimensional H and Ps atoms. The energy difference between the  $\text{Ps}(1)$  formation and the  $\text{H}(2)$  target excitation thresholds is generally named as the Ore gap [3], where only the elastic and  $\text{Ps}(1)$  formation processes compete. Both the direct annihilation (during scattering) and indirect annihilation (through Ps formation) between positron and electron are omitted considering the fact that the lifetime of Ps atoms (0.125 and 140 nanoseconds for para- and ortho-Ps, respectively [3]) is much longer than the scattering time (femtoseconds).

The evolution of the system is determined by solving the TDSE in two spatial degrees of freedom with respect to  $x_1$  and  $x_2$ .

$$i\frac{\partial}{\partial t}\Psi(x_1, x_2, t) = H\Psi(x_1, x_2, t). \quad (4)$$

The initial system wave function is expressed as a product of the electron and positron wave functions at  $t = 0$ ,

$$\Psi(x_1, x_2, t = 0) = \frac{1}{(2\pi\sigma^2)^{1/4}} e^{-\frac{(x_1-x_0)^2}{4\sigma^2}} e^{ik_0x_1} \psi_1(x_2), \quad (5)$$

where  $\psi_1(x_2)$  is the ground state wave function of the H atom with an eigenenergy of  $-0.66982$ , and the positron wave function is represented by a Gaussian wave packet with an initial momentum  $k_0$ . The positron is initially placed at,  $x_0 = -400$  which is far away from the H atom before the collision. For the Gaussian wave packet,  $\sigma = 30$  is used throughout the calculations, which gives an energy width of [31] and a momentum width of  $\Delta k = 1/(\sqrt{2}\sigma) \approx 0.024$ .

The system wave function is propagated by applying the split-operator fast Fourier transform technique. A detailed account of this method is available elsewhere [35, 60]. The wave function evolves on a square grid defined by  $|x_{1,2}| \leq 800$  with space and time steps equal to 0.4. This spatio-temporal discretization yield converged results for all scattering processes investigated in this work. To prevent nonphysical

reflection of the wave function at the grid boundaries, we employ an absorbing masking function [61] at  $x_{\max} = 800$ ,

$$M(x) = \begin{cases} 1 & |x| \leq x_a \\ \cos^{1/8} \left( \frac{\pi}{2} \frac{|x| - x_a}{x_{\max} - x_a} \right) & x_a < |x| \leq x_{\max} \\ 0 & |x| > x_{\max}, \end{cases} \quad (6)$$

for both, the positron and electron wave functions. This ensures that the final scattered positron and electron as well as the formed Ps atom are far away from the nucleus and therefore can be treated as free particles. The absorber width ( $x_{\max} - x_a$ ) is generally set to 20. The probability density distributions of the positron and electron at time  $t$  are obtained, respectively, by

$$\rho(x_1, t) = \int_{-\infty}^{+\infty} |\Psi(x_1, x_2, t)|^2 dx_2 \quad (7)$$

and

$$\rho(x_2, t) = \int_{-\infty}^{+\infty} |\Psi(x_1, x_2, t)|^2 dx_1. \quad (8)$$

In order to get the final populations of the system in different reaction channels, we expand the system wave function on basis sets centered on both the H and Ps atoms [39].

$$\begin{aligned} \Psi(x_1, x_2) = & \sum_{n=1}^{\infty} \int_{-\infty}^{+\infty} b_n(k) \psi_n(x_2) \frac{1}{\sqrt{2\pi}} e^{ikx_1} dk \\ & + \sum_{n=1}^{\infty} \int_{-\infty}^{+\infty} c_n(k) \phi_n(x_2 - x_1) \frac{1}{\sqrt{2\pi}} e^{ik \frac{x_1 + x_2}{2}} dk, \end{aligned} \quad (9)$$

where  $\psi_n(x)$  and  $\phi_n(x_2 - x_1)$  are the eigenstates of the H and Ps atoms, respectively, and the two summations run over all bound and continuum states. Generally speaking, the H and Ps eigenstates are not orthogonal with each other at finite times, and therefore the above two-center expansion is overcomplete on account of the completeness of each basis set. However, after a sufficiently long propagation time, the scattered positron and Ps atom are far away from the target, and these two basis sets can be approximately orthogonal. The expansion coefficients in the target excitation and Ps formation channels are calculated by the projections

$$b_n(k) = \iint \psi_n(x_2) \frac{1}{\sqrt{2\pi}} e^{-ikx_1} \Psi(x_1, x_2) dx_1 dx_2 \quad (10)$$

and

$$c_n(k) = \iint \phi_n(x_2 - x_1) \frac{1}{\sqrt{2\pi}} e^{-ik \frac{x_1 + x_2}{2}} \Psi(x_1, x_2) dx_1 dx_2. \quad (11)$$

The probability of target excitation (Ps formation) in the  $n$ th state with the final positron momentum  $k$  is given by  $|b_n(k)|^2$  ( $|c_n(k)|^2$ ). We note that  $k$  runs from negative infinity to positive infinity, where the negative values represent the reflection of

the scattered positron or the formed Ps atom. By integrating over  $k$ , we obtain the final probabilities for the elastic or target excitation channels

$$I_{H(n)} = \int_{-\infty}^{+\infty} |b_n(k)|^2 dk, \quad (12)$$

and probabilities for the Ps( $n$ ) formation channels

$$I_{Ps(n)} = \int_{-\infty}^{+\infty} |c_n(k)|^2 dk. \quad (13)$$

The probabilities in the direct ionization channel (i.e. three-body breakup, which is different from the electron-loss channel by omitting Ps formation) is estimated by subtracting the populations in all bound states of the H and Ps atoms from one.

$$I_{\text{ion}} = 1 - \sum_{n=1}^{n_{\max}} (I_{H(n)} + I_{Ps(n)}). \quad (14)$$

In numerical computations, we reach converged ionization probabilities by gradually increasing  $n_{\max}$  to large enough values.

Besides the transition probabilities, we are also interested in the total transmission ratio of the positron in the scattering process

$$T_t = \frac{\sum_{n=1}^{n_{\max}} \left( \int_0^{+\infty} |b_n(k)|^2 dk + \int_0^{+\infty} |c_n(k)|^2 dk \right)}{\sum_{n=1}^{n_{\max}} \left( \int_{-\infty}^{+\infty} |b_n(k)|^2 dk + \int_{-\infty}^{+\infty} |c_n(k)|^2 dk \right)}, \quad (15)$$

which, to the best of our knowledge, has not been investigated until now. The total reflection ratio can be obtained by subtracting  $T_t$  from one. The transmission ratio in the channel leaving the target atom in the  $n$ th state after the collision is given by

$$T_{H(n)} = \frac{\int_0^{+\infty} |b_n(k)|^2 dk}{\int_{-\infty}^{+\infty} |b_n(k)|^2 dk}. \quad (16)$$

Likewise, the transmission ratio for the Ps formation in the  $n$ th state is

$$T_{Ps(n)} = \frac{\int_0^{+\infty} |c_n(k)|^2 dk}{\int_{-\infty}^{+\infty} |c_n(k)|^2 dk}. \quad (17)$$

### 3. Results and discussion

#### 3.1. Interference between incident and reflected positrons

The time evolutions of the probability density distributions for the electron and positron during the positron-H scattering are shown in figures 1(a) and (b), respectively, for an incident energy of  $E_0 = 0.40$ , i.e.  $k_0 = 0.894$ . For this intermediate impact energy, the elastic and Ps(1) formation channels are fully open, while the H(2) excitation channel is just open. From figure 1(a), it is clearly seen that although most of the electron density remains localized near the nucleus, i.e., in the

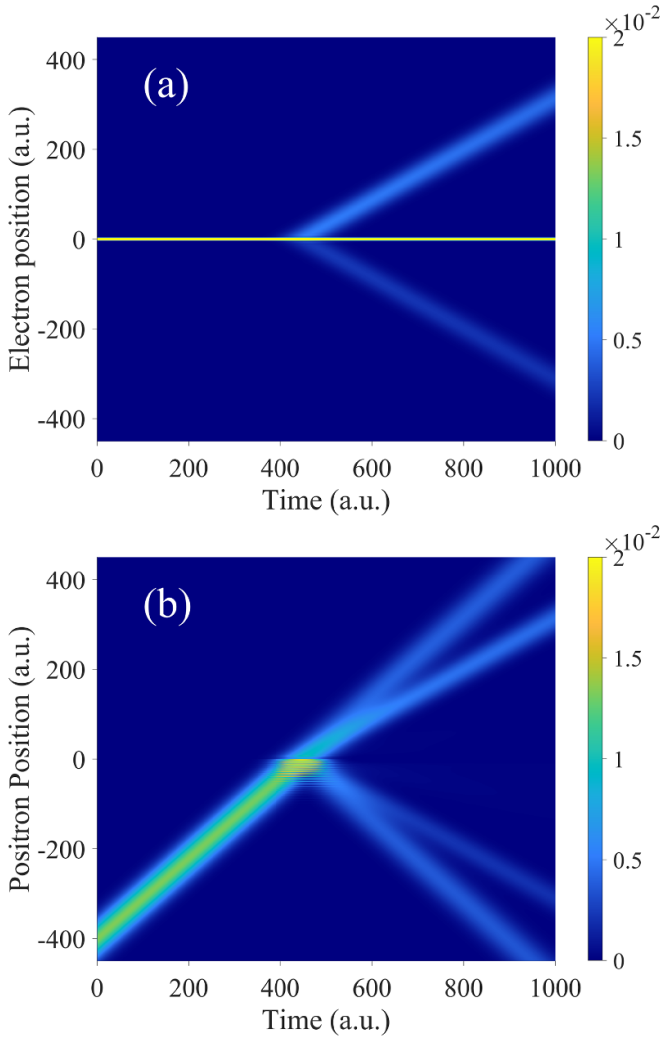


**Figure 1.** Probability density distributions of (a) electron and (b) positron as a function of time during the collision. The positron incident energy is 0.40, and the initial center of the incident positron wave packet is placed at  $x_1 = -400$ . The forward and backward scattered trajectories in (a) and the inner two trajectories in (b) represent the Ps formation.

elastic channel, there exist two scattered electron wave packets that move outward with the same speed in opposite directions. The upper and lower parts represent, respectively, the forward and backward scattering of electrons induced by the energetic positron. Due to energy conservation, forward and backward scattering occur at the same speed. A similar picture of the time evolution of the positron probability density distribution is displayed in figure 1(b). The positron moves along a straight line towards the H atom with momentum  $k_0$  before the collision, and after scattering, it splits into four components, with the outer two wave packets representing elastic forward and backward scatterings and the inner two wave packets indicating the forward and backward Ps formations. From the comparison between figures 1(a) and (b), it can also be found that the inner scattered positrons have the same speed as the scattered electrons. Calculating the time evolution of the system wave function by solving the TDSE thus allows the spatio-temporal resolution of different reaction channels. Due

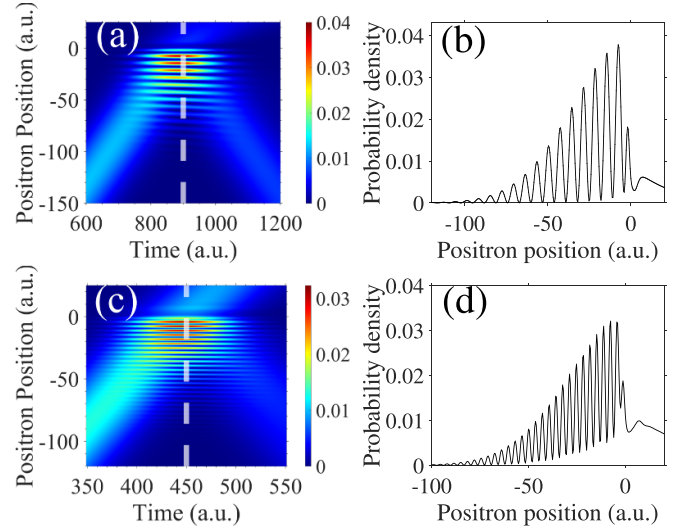


**Figure 2.** Positron probability density distributions for (a) 0.10 and (c) 0.40 incident energies. (b) and (d) are the snapshots of density distributions at the time indicated by the white dashed lines on the left panels. (b) Snapshot time at  $t = 900$  and (d) snapshot time at  $t = 450$ . Interference fringes between the incident and reflected positron wave packets are clearly displayed near the collision center at  $x_1 = 0$ .

to energy conservation, there is no positron probability density left near the H atom, although in the present one-dimensional model the system does support the formation of a stable three-body bound state (we will revisit this topic in Section 3.4).

Besides the asymptotic motion of the positron before and after scattering, we observe in figure 1(b) strong interference fringes in the reaction region. For a better view of the interference pattern, we draw in figures 2(a) and (c) the time evolution of the positron density distribution for incident energies of 0.10 and 0.40, respectively. At  $E_0 = 0.10$  only elastic positron scattering happens, while at  $E_0 = 0.40$  an additional Ps(1) formation channel opens. It is clearly observed from the comparison that the spatial oscillation of the positron density distribution is significantly enhanced with increasing the incident energy. This standing-wave pattern can be attributed to the interference effect between the incident and reflected positron wave packets, i.e. the positron wave packet first collides with and then reflects off the nucleus, meanwhile interfering with the non-collisional part of the wave packet.

The interference structure can be analyzed within a plane-wave approximation for both the incident and reflected positrons. We account for a phase shift of  $\pi$  of the reflected positron wave, since waves accumulate a phase shift of  $\pi$  upon reflection off a denser material [62]. When the energy of the incident positron is relatively high, considering the short-range character of the soft-core Coulomb potential and the fast scattering process, we can ignore the long-range character of all Coulomb interactions and treat the nucleus as a potential well of finite height and vanishing width. The incident positron wave function can then be approximated by a plane wave with amplitude  $f$  and constant momentum  $k_0 = \sqrt{2E_0}$ , i.e.  $\chi_i(x_1, t) = f e^{ik_0 x_1} e^{-iE_0 t}$ . Upon reflection, the positron reverses its direction with an additional phase  $\pi$  and

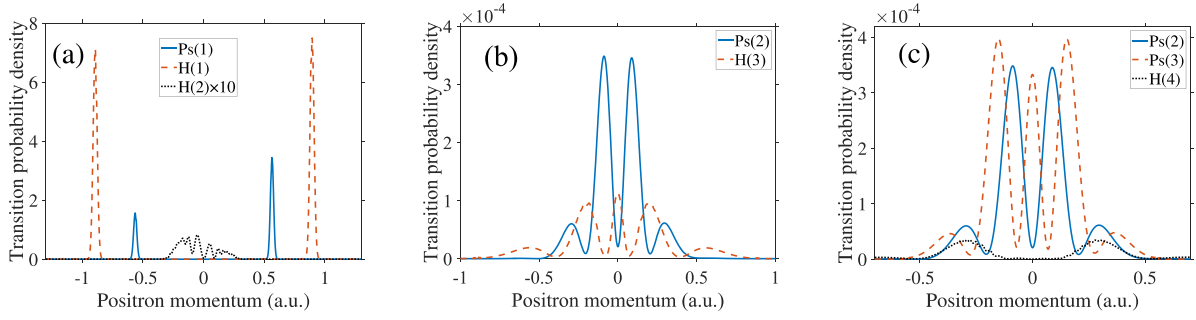


**Figure 3.** The transition probability density distributions in different reaction channels as a function of the final momentum of the scattered positron for an incident positron energy of  $E_0 = 0.40$ . In panel (a),  $|b_1(k)|^2$ ,  $|b_2(k)|^2$ , and  $|c_1(k)|^2$  represents the H(1), H(2), and Ps(1) channels, respectively. Panels (b) and (c) are similar to (a), but for the Ps(2), H(3) and Ps(2), Ps(3), H(4) scattering channels, respectively.

changes its amplitude to  $g$ , i.e.  $\chi_r(x_1, t) = g e^{-ik_0 x_1 - i\pi} e^{-iE_0 t}$ . Therefore, the superposition of the positron wave packet in the scattering region is given by

$$\chi(x_1, t) = [f e^{ik_0 x_1} + g e^{-ik_0 x_1 - i\pi}] e^{-iE_0 t}. \quad (18)$$

The corresponding probability density reads

$$\rho(x_1, t) = |\chi(x_1, t)|^2 = f^2 + g^2 - 2fg \cos(2k_0 x_1), \quad (19)$$

which reveals a time-independent oscillatory structure with period  $\pi/k_0 = \pi/\sqrt{2E_0}$ . The profiles of the interference fringes in figures 2(b) and (d) agree perfectly with the periodic structure obtained from the above formula. If Coulomb interactions between the positron and target atom are taken into account, the incident and reflected positron wave packets cannot be treated as plane waves, and the energy of the reflected positron also changes. In this case, the interference pattern is distorted as time evolves [63]. Nevertheless, we find that the phase-jump approximation works very well for a wide range of incident energies, even as low as  $E_0 = 0.10$ . As a consequence of the interference effect and strong repulsion of the soft-core Coulomb potential, a minimum appears in the positron probability density at  $x = 0$ . This is consistent with our finding in figure 1(b) that the scattered positron cannot be bound by the one-dimensional H atom.

### 3.2. Critical behavior near the channel-opening thresholds

The transition probability density distributions of the positron–H scattering system at  $E_0 = 0.40$  are shown in figure 3 for those reaction channels listed in equation (3). The probabilities for the target excitation and Ps formation are calculated using equations (10) and (11), respectively. The horizontal axes of these figures represent the momentum of the scattered positron, which is to say, for the Ps formation channels we scale the final momentum of the Ps atom by 1/2 to facilitate a direct comparison between the H(n) and Ps(n) channels. Figure 3(a) displays the probabilities of the H(1), Ps(1), and H(2) open channels for both positive and negative positron momenta. The peak positions of the H(1) elastic and the Ps(1) formation channels follow the energy conservation law, and these four peaks in the momentum space

correspond exactly to the four scattered wave packets in the spatial probability density distributions shown in figure 1(b). Both of these two processes slightly prefer forward scattering over backward scattering at this incident energy. The H(2) excitation probabilities, however, are much smaller than those of H(1) and Ps(1), and exhibit drastic oscillations at small momenta. This is due to the fact that the central energy of the incident positron wave packet lies above, but very close to, the channel opening threshold ( $E_{\text{th}}^{\text{H}(2)} = 0.395$ ). It is interesting to observe that for such a just-opened excitation channel, the positron prefers backward scattering. This is consistent with the intuitive expectation that, within a one-dimensional scattering model, the positron cannot easily transfer across the proton.

Due to the finite energy width of the positron Gaussian wave packet, higher-lying reaction channels can also be opened, even though the central incident energy lies below corresponding thresholds. The transition probabilities in the Ps(2), H(3), Ps(3), and H(4) channels at  $E = 0.40$  are displayed in figures 3(b) and (c). The probabilities of these weak scattering processes are generally several orders of magnitude smaller than those of fully-opened channels, since only a small (high-energy) portion of the positron wave packet participates in these reactions. More interestingly, the comparison between different channels reveals drastic but complementary oscillations in, e.g., the Ps(2) and H(3) and the Ps(2) and Ps(3) channels. Such an oscillation structure was first observed by Larkin et al [39], however, as far as we know its underlying physics has not been clearly tracked. In what follows, a qualitative explanation of this phenomenon is provided tentatively.

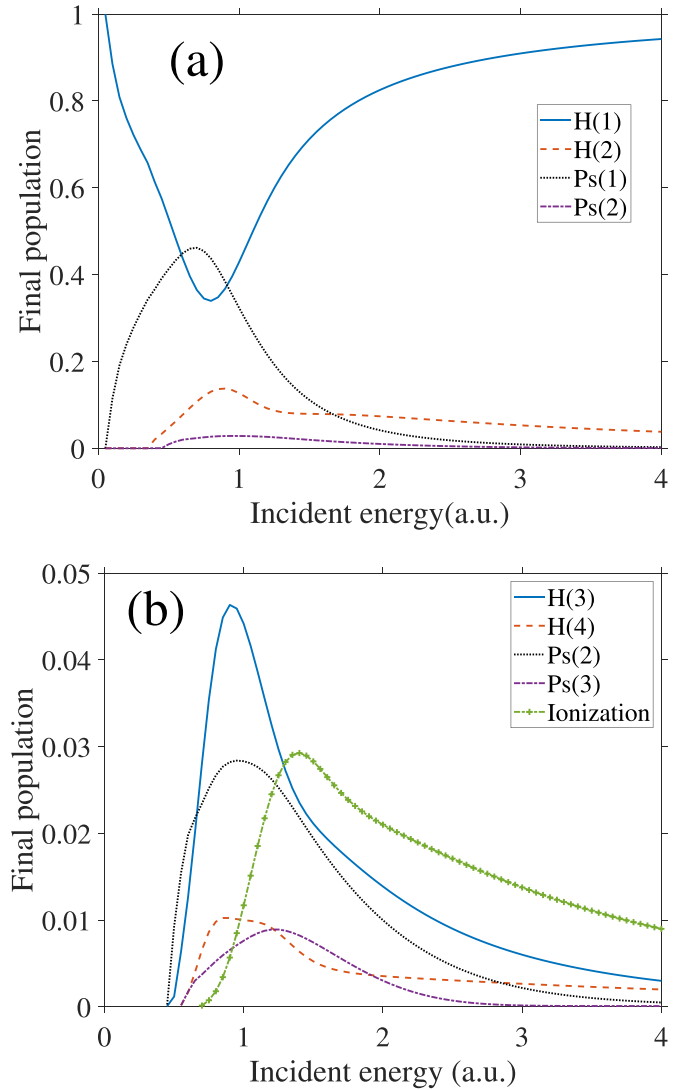
Let us first focus on the probabilities at zero momentum, which correspond to the ideal situation that the positron remains near the nucleus in both target excitation and Ps formation channels, i.e., the positron incident energy strictly equals the channel opening threshold. In this case, the centers of the target H atom and the formed Ps atom coalesce, and the electron transfers directly from the initial H(1) ground state to either H(n) or Ps(n) states (i.e. the center of the electronic wave function does not move). Since in the one-dimensional model, both H(n) and Ps(n) states have a one-to-one correspondence between the quantum number  $n$  and spatial parity  $P = (-1)^{n+1}$  [59], transitions from the initial even ground

state to even final states are allowed, whereas transitions to all odd-parity states tend to be suppressed [64]. As one can see from figure 3, the probabilities in H(2), Ps(2), and H(4) channels at zero momentum are minimal, while the probabilities for H(3) and Ps(3) peak. When the final momentum of the scattered positron is increased, the initial electronic wave function dynamically transits into either Ps( $n$ ) channels, by changing its center position, or the H( $n$ ) channels, due to energy transfer from the incident positron. In both cases, the system parity is not preserved. Nevertheless, a strong parity propensity rule at specific values of positron momentum can still be observed: peaks and valleys appear alternatively in channels with different parities. The competitive oscillation also exists in higher-lying H( $n$ ) and Ps( $n$ ) channels, which are not shown here due to their extremely small magnitudes. We therefore conclude that the oscillatory structures in the probabilities of target excitation and Ps formation channels are due to the strong competition between channels with near threshold energies but different parities.

### 3.3. Populations and positron transmission ratios

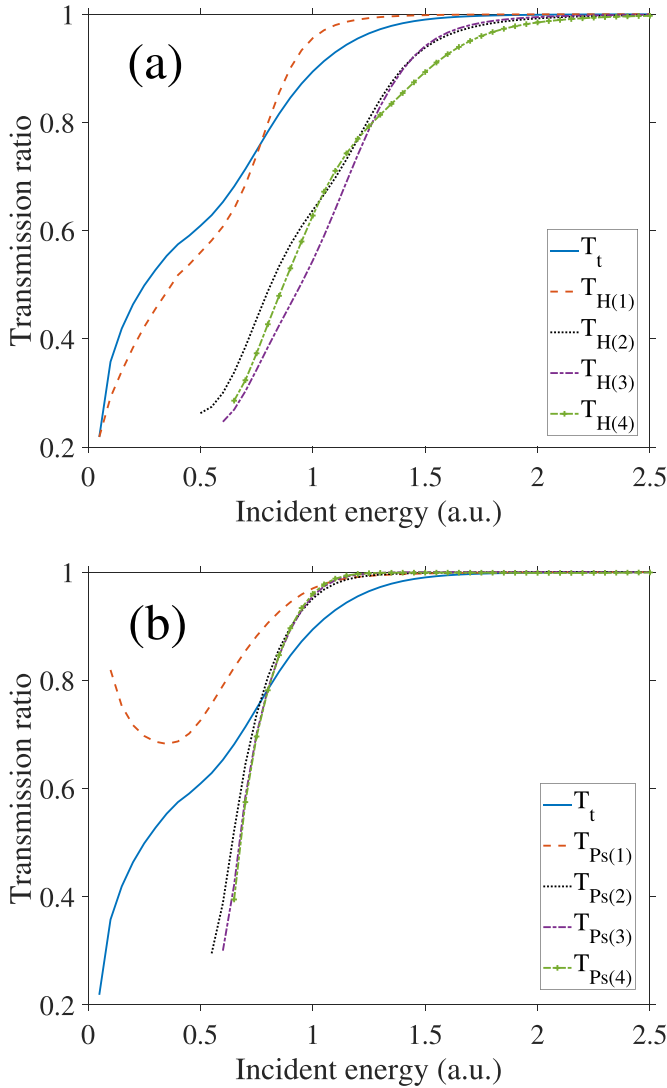
In figures 4(a) and (b), we show the final populations of the scattering system in different reaction channels for positron incident energies increasing up to 4. Our results for  $E_0 < 1$  are indistinguishable from the previous calculations of Larkin *et al* [39] in the present figure scale. We further calculated the population in the direct ionization channel by employing equation (14), where the largest quantum number of the bound states  $n_{\max}$  is gradually increased to 15 to ensure that the difference between results using  $n_{\max}$  and  $n_{\max} - 1$  is invisible within the figure scale. The populations in inelastic reaction channels at corresponding channel-opening thresholds are in principle not zero because of the finite energy width of the incident positron. Nevertheless, they are omitted in the figures due to their negligible magnitudes.

Figure 4(a) shows that, in the Ore gap, where only the elastic and Ps(1) formation channels are open, the Ps(1) population increases rapidly as the incident energy increases. This leads to fast dissipation of the electron population in the initial ground state. When higher-lying inelastic channels are open, the increase of the Ps(1) channel population slows down and reaches a maximum at an energy of about 0.690, where its population is almost two times larger than in all other inelastic channels. This maximum position is nearly identical to the target ionization threshold (0.670) and, somewhat surprisingly, consistent with full three-dimensional positron–hydrogen scattering, where the Ps(1) formation cross section has a maximum exactly at the H(1) ionization threshold [7]. When the positron incident energy increases to 2, the population in the Ps(1) channel becomes less than 0.050 and continuously diminishes with further increasing incident energy. In this high-energy region, the positron moves fast across the target atom, and the brief interaction with the electron leads to a small probability for the positron to capture an electron from the target. In fact, most of the electron probability density remains bound in the ground state of the H atom.



**Figure 4.** Final populations of the scattering system as a function of the positron incident energy. Populations in the (a) H(1), Ps(1), H(2), and Ps(2) and (b) Ps(2), H(3), Ps(3), H(4), and ionization channels.

In figure 4(b) an interesting observation is the similar behavior and comparable magnitude of the populations in neighboring channels with similar threshold energies. For example, the Ps(2) and H(3) channel populations generally have the same maximum position and variation trend, except that the peak magnitude in the latter is two times larger than that in the former. The Ps(3) and H(4) channel populations are comparable in the maximum magnitude, but peak at different positions. Another common behavior between the Ps( $n$ ) formation and H( $n + 1$ ) excitation channels is that at high incident energies the Ps formation population decreases much faster than the target excitation population. The same is true between the Ps(1) and H(2) reaction channels displayed in figure 4(a). This is qualitatively consistent with three-dimensional positron–atom scattering at high impact energies, where the target excitation cross sections are much larger than the Ps formation cross sections [7, 20]. Due to the limitations of the one-dimensional model employed here, we



**Figure 5.** Transmission ratios of the positron in the lowest several reaction channels as a function of the incident energy. Transmission ratios in the (a) H(1), H(2), H(3), and H(4) and (b) Ps(1), Ps(2), Ps(3), and Ps(4) channels. The total transmission ratio  $T_t$  is included in both graphs for comparison.

are not in a position to make direct comparisons with the three-dimensional positron–H scattering cross sections. These qualitative similarities between the one-dimensional model and the real three-dimensional system is encouraging for our future laser-assisted positron–atom investigations in reduced dimensionality.

The transmission ratios of the positron in various reaction channels and the total transmission ratio are shown in figure 5. The total ratio  $T_t$  increases monotonically as the incident energy increases and saturates at about  $E_0 = 1.50$ . This can be understood from the fact that the positron has a larger probability to penetrate through the target atom with higher initial kinetic energy. The transmission ratio in the elastic scattering channel  $T_{H(1)}$  generally follows the same behavior as  $T_t$  due to its dominant role over other channels in almost the entire energy region, as one can derive from the populations shown in figure 4(a). The

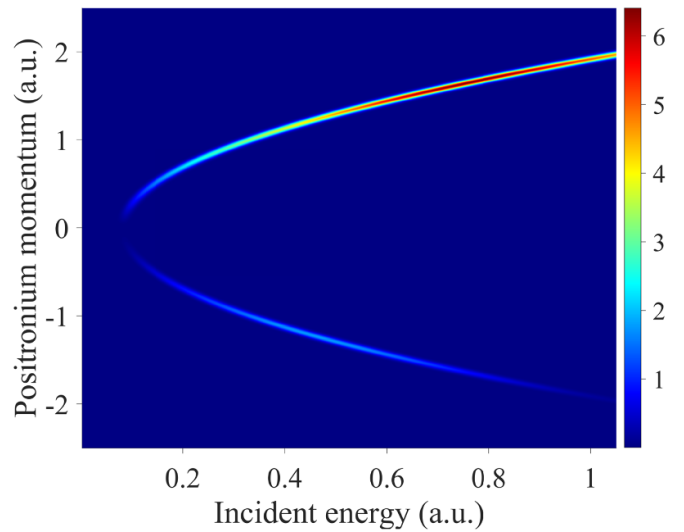


**Figure 6.** Transition probability density distribution  $|c_1(k)|^2$  in the Ps(1) formation channel as a function of the final positronium momentum  $k$  and the positron incident energy  $E_0$ . The vertical axis indicates the momentum of the formed Ps(1) atom, where positive and negative values represent forward and backward scattering, respectively.

ratios in various target excitation channels show quite similar trends and gradually increase from 0.250 to one as the incident energy increases from corresponding channel-opening thresholds to about 2. The comparison between  $T_{H(1)}$  and  $T_{H(n \geq 2)}$  shown in figure 5(a) demonstrates that in the entire energy region the incident positron is more likely to be reflected in the excitation channels than in the elastic channel.

The transmission ratios in the Ps formation channels are displayed in figure 5(b), where the total ratio is also included for comparison. The transmission ratio for Ps formation in the ground state  $T_{Ps(1)}$  shows a distinct behavior from the total ratio  $T_t$  and those of Ps formation in excited states  $T_{Ps(n \geq 2)}$ . In the Ps(1) channel, the formed Ps atoms always prefer forward scattering, even for incident energies that just exceed the channel-opening threshold, although at such low incident energies most of the positron wave packet will be reflected by the target atom ( $T_t \approx 0.3$ ). The large positron transmission ratio in the Ps(1) channel is probably related to the low channel-opening threshold energy, which still warrants further consideration. We note that a similar phenomenon was predicted in the three-dimensional positron–H scattering based on the distorted-wave theory, where the Ps(1) differential cross section strongly peaks at forward scattering [25]. For a better view of the forward and backward scattering dynamics, we show in figure 6 the transition probability density distributions in the Ps(1) formation channel. We find that for all incident energies Ps atoms are more likely formed with positive momenta. The forward scattering probability, which peaks at about  $E_0 = 0.750$  and  $k_{Ps} = \sqrt{4(E - 0.082)} = 1.635$  with a magnitude of about 6, is generally three times larger than the backward scattering probability, which peaks at about  $E_0 = 0.450$  and  $k_{Ps} = -1.213$  with a magnitude smaller than 2. For



incident energies above 1, the Ps formation in the backward direction can hardly be observed.

In both figures 5(a) and (b), we only show the transmission ratios for incident energies exceeding the corresponding thresholds. Results for energies smaller than the threshold energies do not appear to follow a general trend. The results for  $T_{Ps(n \geq 2)}$  shown in figure 5(b) share a common monotonic trend that is similar to the collective behavior of  $T_{H(n)}$  displayed in figure 5(a), except that  $T_{Ps(n)}$  increases much faster than  $T_{H(n)}$  with increasing the incident energy. In other words, the probabilities of Ps formation in backward scattering diminish much faster than the probabilities of target excitation in the same direction. This is, at least partially, responsible for our finding in figure 4 that the final populations in the Ps formation channels decrease faster than those in the target excitation channels.

### 3.4. Positron–hydrogen bound states in reduced dimensionality

The bound states of three-body systems in reduced-dimensionality models have attracted considerable attention in recent years [65–68]. In this subsection, we will discuss the possible three-particle bound-state formation in the composite positron–hydrogen system. It is well-known that in full dimensionality a positron cannot be attached to the hydrogen atom and form a stable bound system [69–71]. However, it is still unclear if such a bound state would exist in the reduced-dimensionality model with soft-core Coulomb potentials. To find the eigenenergies of the three-body system with the Hamiltonian in equation (1), we solve the TDSE with an imaginary-time propagation method [72]. The initial wave functions for the positron and electron are Gaussian wave packets, both centered at the origin. Different initial conditions have been tried to remove possible spurious solutions. Our simulations predict a converged ground state  $e^+H(1)$  with an energy of  $-0.702$  and an excited state  $e^+H(2)$  with energy  $-0.682$  for the positron–hydrogen system. These two states are slightly lower than the ground state energies of the Ps atom ( $-0.588$ ) and H atom ( $-0.670$ ), and therefore stable against dissociation.

The wave functions of the ground and excited states of the  $e^+H$  system are shown in figures 7(a) and (b), respectively. Compared to the  $H^-$  ion in the same one-dimensional model [73], a distinct feature of the  $e^+H$  ground state wave function is the lack of antisymmetrization with respect to changing coordinates of the electron and positron. As a result, the system wave function has only spatial inversion symmetry, i.e.  $\Psi(x_1, x_2) = \Psi(-x_1, -x_2)$ . It can also be observed from both figures 7(a) and (b) that the spatial extension of the positron wave function is much larger than that of the electron. This can be clearly seen in figure 7(c), where the probability density distributions of the positron and electron in the  $e^+H$  ground and excited states are displayed separately. The electron density distribution in the  $H(1)$  atom is also included for comparison. It is found that in the positron–hydrogen bound states, the positron probability densities are localized at the two sides of the nucleus due to the repulsive interaction between them. Compared to the electron in the  $H(1)$  state, the electron in the

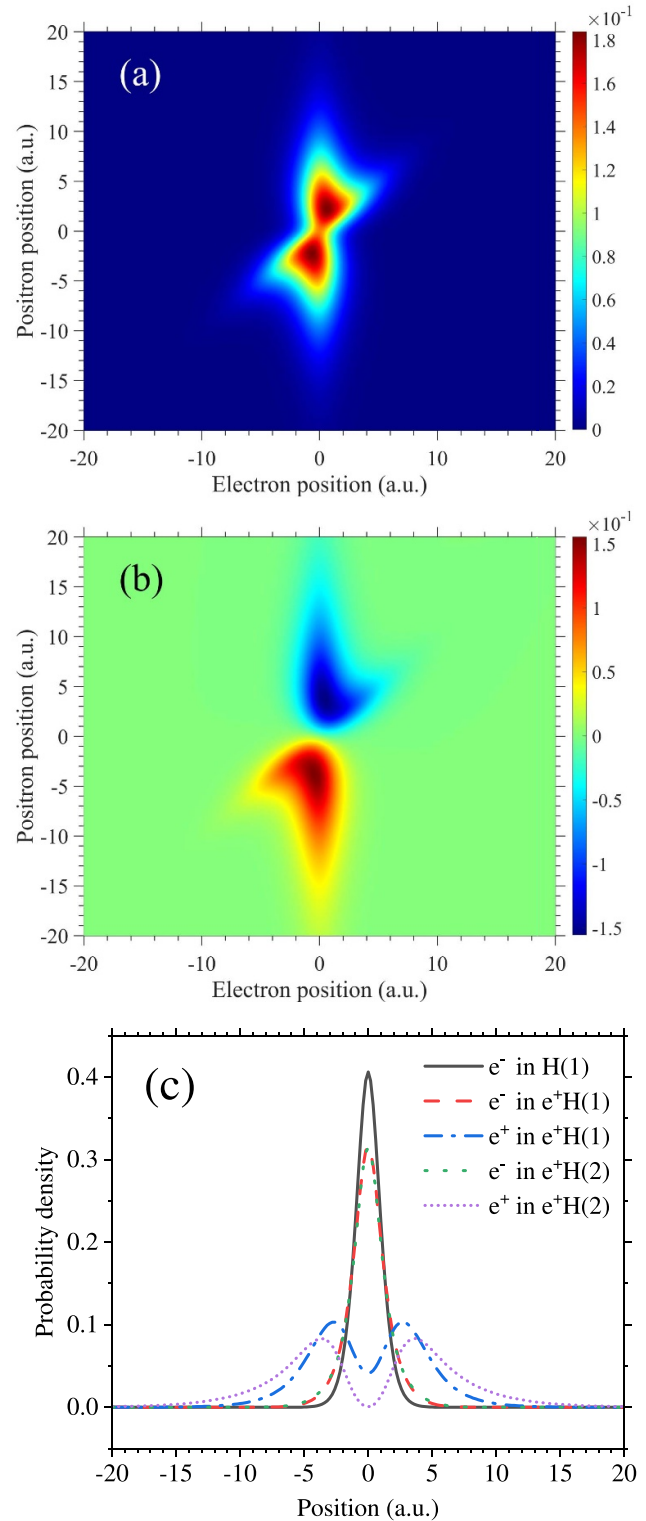


**Figure 7.** Contour plots of wave functions for (a) the ground state and (b) the excited state of the positron–H system in the reduced-dimensionality model. (c) Comparison of the probability density distributions for the electron and positron in the  $e^+H(1)$  ground and  $e^+H(2)$  excited states of the  $e^+H$  system, and the electron in the ground state of the H atom.

$e^+H$  system is slightly displaced from the origin to balance the attractive electron–nucleus and electron–positron interactions and screen the positron–nucleus repulsive interaction. On

average, the positron in the excited state of  $e^+H$  is located further away from the nucleus than in the ground state, while the electron distribution does not change much.

Since the energies of the positron–hydrogen bound states are lower than the ground state energy of the H atom in the present reduced-dimensionality model, the formation of three-body bound states is energetically prohibited in the non-radiative scattering process. However, when the system is exposed to an assisting laser field, does radiative stabilization into these bound states become possible? To address this question it is worth noting that the use of an intense laser field would tend to break up the H and Ps atoms as well as the three-body bound states. On the other hand, application of a linearly-polarized laser field with its polarization direction parallel to the initial momentum of the positron would significantly confine the motion of electron and positron to the polarization direction [58]. It should thus be well represented by a one-dimensional model that, upon radiative stabilization, would support a three-body bound state.

Next, we investigate the modulation effect of an assisting linearly-polarized laser field with the wavelength of  $\lambda = 800$  nm (frequency  $\omega = 0.057$ ) on the formation of three-body bound states during the positron–H atom scattering. The total Hamiltonian of the laser-assisted scattering system is

$$H_L = H + V_L, \quad (20)$$

where the laser-free atomic Hamiltonian  $H$  is given by equation (1), and  $V_L$  represents the laser–atom interaction. In the dipole approximation, the interaction between the laser field and the incident positron and target electron in the length gauge is expressed as

$$V_L(x_1, x_2, t) = E(t)(x_2 - x_1), \quad (21)$$

in which the electric field  $E(t)$  is obtained from the vector potential  $A(t)$  through  $E(t) = -dA(t)/dt$ . The vector potential employed in this work reads

$$A(t) = A_0 f(t) \cos[\omega(t - t_0) + \varphi], \quad (22)$$

where  $\varphi$  is the carrier-envelope phase and  $f(t)$  is the envelope function in the form

$$f(t) = \begin{cases} \sin^2\left(\frac{\pi}{2} \frac{t}{\tau_R}\right) & 0 < t < \tau_R \\ 1 & \tau_R < t < \tau - \tau_R \\ \cos^2\left(\frac{\pi}{2} \frac{t - 3\tau_R}{\tau - 3\tau_R}\right) & \tau - \tau_R < t < \tau \\ 0 & \text{else} \end{cases}. \quad (23)$$

In the present work, the pulse duration time  $\tau$  is chosen to be  $5T$ , where  $T (= 2\pi/\omega)$  is the laser optical cycle. The ramp on and off time duration  $\tau_R$  is a quarter of the total pulse duration, i.e.  $\tau_R = \tau/4$ .

For a positron incident energy of 0.05 and peak laser intensity of  $2 \times 10^{13} \text{ W cm}^{-2}$ , the variation of the positron probability density as a function of propagation time is shown in figure 8(a). Despite the complicated modulation effect of the laser field on the scattering process, it is clearly observed that

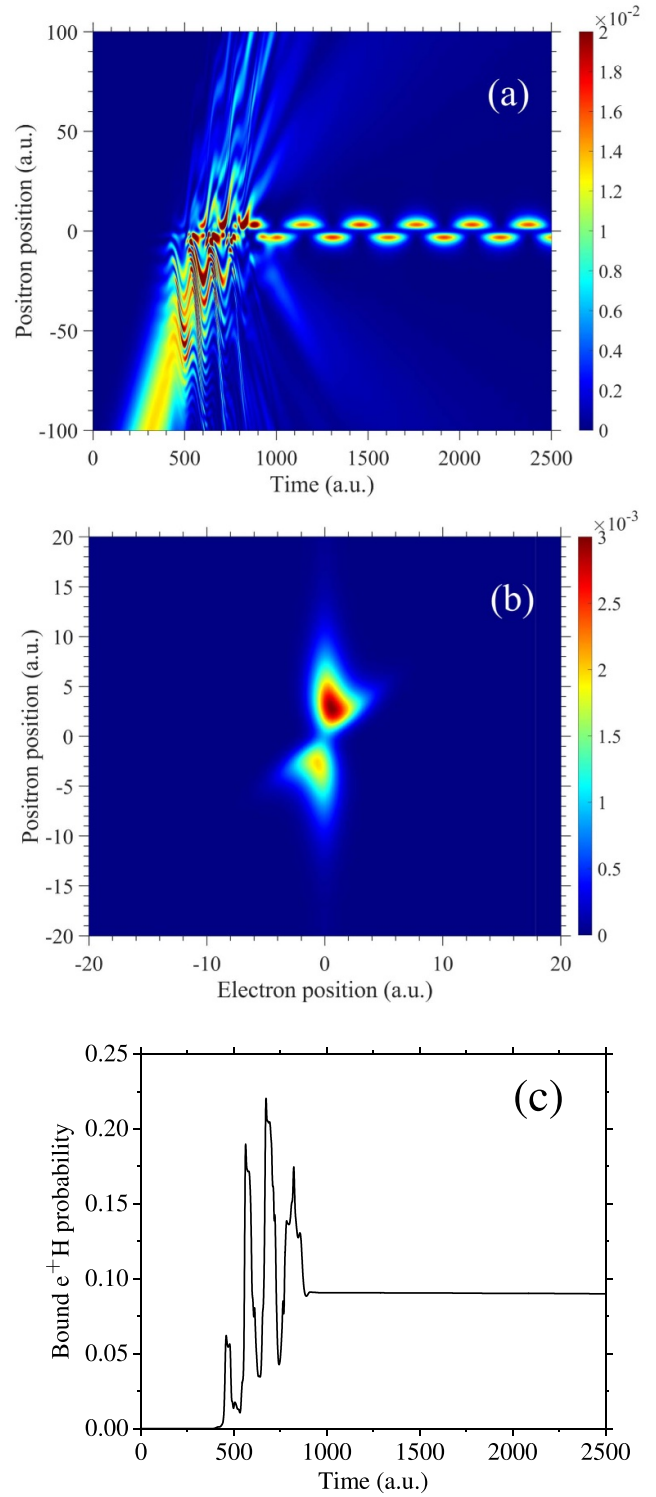


**Figure 8.** (a) The positron probability density as a function of time. The positron incident energy is 0.05, and the laser intensity is  $2 \times 10^{13} \text{ W cm}^{-2}$ . (b) Instantaneous ( $t = 1400$ ) probability density distribution of the  $e^+H$  bound state during the positron–hydrogen collision. This state is a superposition of the ground and excited states of the  $e^+H$  system. (c) Population of the  $e^+H$  bound state as a function of time.

the positron wave packet splits into three parts after the collision: a forward scattering part, a reflected wave packet, and a trapped part. The trapped positron remains localized in the

vicinity of the nucleus and forms a bound state with the target H atom, however, with its density distribution oscillating at a constant frequency. In the Supplementary Material, we provide a video depicting the time evolution of the spatial density distribution of the scattering system during the collision by fixing the view at the origin. The formation of  $e^+H$  bound state and the oscillation in density distribution can be clearly observed. A snapshot of the spatial density distribution at  $t = 1400$  (a long enough time after the collision) is shown in figure 8(b). It can be seen that both the positron and electron are generally restricted into the configuration space of  $|x_{1,2}| \leq 10$  and mainly distributed in the first and third quadrants. This is consistent with our imaginary-time calculations of the ground and excited states of the  $e^+H$  system (see figure 7 for the corresponding density distributions). Our further analysis shows that the probability density of the three-body bound states oscillates with a period of  $t_b = 315$ , which corresponds to a frequency of  $\omega_b = 0.02$ . This is identical to the energy difference between the ground and excited states of the  $e^+H$  system. We therefore conclude that the three-body bound state formed in the laser-assisted positron-H scattering is a superposition of the ground and excited states of the composite  $e^+H$  system, and the oscillation in the density distribution originates from the coherence between these two eigenstates.

Figure 8(c) displays the variation of population for the  $e^+H$  bound-state formation as a function of evolution time, with the same incident energy and laser parameters as used in figure 8(a). Within the time frame of  $500 < t < 1000$ , where the Coulomb interaction between the incident positron and the target H atom as well as the positron- and electron-laser interactions are strongest and compatible in strength, three-body bound-state formation is significantly enhanced and modulated by the assisting laser field. In the present case, up to a quarter of the positron probability density can be transiently accommodated into the bound state during the collision. When the laser field is turned off and after the system propagates freely for a sufficiently long time, the final population of the three-body states stabilizes at about 0.09.

It is obvious that the three-body bound-state formation in the laser-assisted positron-H scattering depends closely upon both the positron incident energy and the laser parameters. In figure 9(a), we present the formation probability of the  $e^+H$  bound state as a function of the laser intensity with the positron incident energy fixed at 0.05. By projecting the final bound state wave function onto the stationary wave functions of the ground and excited states of the  $e^+H$  system, we can further analyze the contribution from each eigenstate. It is surprisingly found that in such low-energy scattering, the formation of the three-body excited state is always preferred over the ground state. When the laser intensity is decreased to  $10^{10} \text{ W cm}^{-2}$ , the modulation effect of the laser field on the scattering process is negligible. Then the  $e^+H$  bound state can hardly be formed, as in the laser-free scattering process. If the laser intensity is high enough, e.g.,  $10^{14} \text{ W cm}^{-2}$ , the intense laser field would directly ionize the H atom (and the formed Ps), with a small

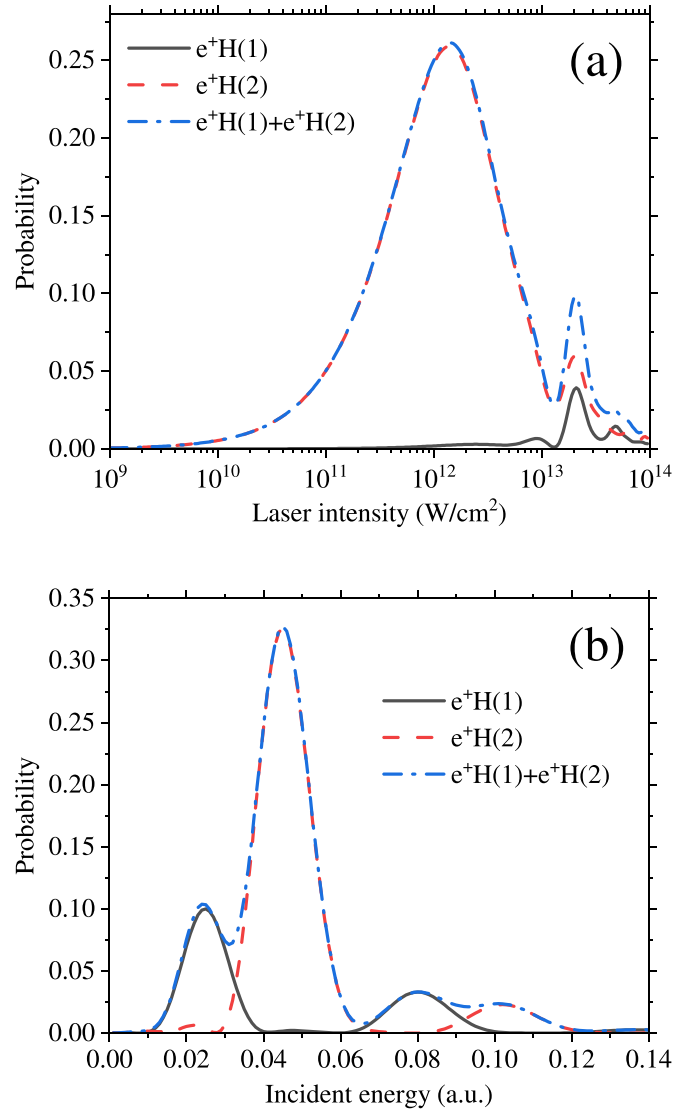


**Figure 9.** (a) The  $e^+H$  bound-state formation probability in the laser-assisted positron-H scattering as a function of the laser intensity. The positron incident energy is fixed at 0.05 and other laser parameters are the same as before. (b) Same as (a) for a fixed laser intensity of  $10^{12} \text{ W cm}^{-2}$  and variable positron incident energy.

probability for the electron and positron to form a three-body bound state. The largest probability under the present laser parameters is achieved at about  $1.4 \times 10^{12} \text{ W cm}^{-2}$ , while the dip at about  $1.3 \times 10^{13} \text{ W cm}^{-2}$  is caused by the strong competition with other inelastic channels (A detailed discussion of the modulation effect of laser field on different reaction channels will be reported elsewhere).

In figure 9(b), we illustrate the formation probability of the  $e^+H$  bound state and the separate contributions from the  $e^+H(1)$  and  $e^+H(2)$  eigenstates, as a function of the positron incident energy. The laser intensity is fixed at  $10^{12} \text{ W cm}^{-2}$ . A total number of four peaks, with two for each eigenstate, are observed in the bound-state formation probabilities. The peak locations are in full agreement with energy conservation.

$$E_0^{e^+} + E^H - n\omega = E_b^{e^+H}, \quad (24)$$

where  $E_0^{e^+}$  and  $E^H$  are the positron incident energy and the ground state energy of the H atom, respectively.  $E_b^{e^+H}$  is the scattering final state (ground or excited eigenstate) energy of the  $e^+H$  system. The integer value  $n$  represents the number of emitted photons with the frequency  $\omega$ . It is easily verified that the first and second peaks in the formation of each eigenstate correspond to the one- and two-photon emissions in the laser-assisted scattering. For each eigenstate, the probability of the second peak is generally one order of magnitude smaller than that of the first peak. The excess energy of the positron–H atom collisional system can be emitted radiatively in the harmonic-order frequencies of the assisting laser field, which enables the production of three-body bound states in the collision.

#### 4. Conclusion

In this work we investigated the quantum dynamics of positron–H atom scattering in a reduced-dimensionality quantum model, where the effective interactions between charged particles are represented by soft-core Coulomb potentials. The time evolution of the system wave function is performed by numerically solving the TDSE. The final populations in different reaction channels are obtained by projecting the system wave function onto channel states. Strong interference fringes between the incident and reflected positron wave packets are observed near the target nucleus. Due to the finite energy width of the incident positron Gaussian wave packet, higher-lying reaction channels are accessible to low-energy incident positron wave packets, even if their central energy lies below the thresholds. We find that in these ideally closed channels, strong competition exists between neighboring channels with similar threshold energies but different spatial parities.

The final populations of the scattering system in various target excitation, Ps formation, and direct ionization channels are calculated in a wide range of incident energies. Our results show good agreement with previous calculations at low energies. The observed faster decrease of the final populations in the Ps formation channels than in target excitation channels with increasing the positron energy is consistent with our intuitive expectation for the three-dimensional physical system. We also investigated the transmission ratios of positron in individual and total scattering channels. An interesting phenomenon is found that only the Ps formation in its ground state prefers forward scattering, while in all other inelastic channels the transmission ratios increase gradually from a small proportion to one.

We identified two stable three-body bound states of the positron–H atom system in the present reduced-dimensionality quantum model. While the formation of three-body bound states is energetically forbidden in non-radiative scattering, our calculation provides evidence that it can be enabled by a moderate-intensity assisting laser field, due to stimulated multi-photon emission. The introduction of an

assisting laser field may thus allow us to control and manipulate the formation of positronic bound states in the positron–atom scattering in the laboratory.

#### Data availability statement

All data that support the findings of this study are included within the article (and any supplementary files).

#### Acknowledgments

This work was supported by the National Key Research and Development Program of China (Grant No. 2022YFE0134200) and the National Natural Science Foundation of China (Grant No. 12174147). U T acknowledges partial support from U.S. National Science Foundation Grant No. PHY 2110633 (probing and controlling electron dynamics) and Chemical Sciences, Geosciences, and Biosciences Division, Office of Basic Energy Sciences, Office of Science, U.S. Department of Energy Award No. DEFG02-86ER13491 (attosecond interferometry).

#### Supplementary material

The supplementary material depicts the time evolution of the spatial density distribution of the laser-assisted positron–H atom scattering with the positron incident energy of 0.05 and laser parameters given in figure 8.

#### Data availability statements

The data that support the findings of this study are available from the corresponding author upon reasonable request.

#### ORCID iDs

Li Guang Jiao  <https://orcid.org/0000-0003-4525-0356>  
 Aihua Liu  <https://orcid.org/0000-0001-6045-001X>  
 Uwe Thumm  <https://orcid.org/0000-0001-9378-6601>  
 Yew Kam Ho  <https://orcid.org/0000-0001-8812-1357>

#### References

- [1] Anderson C D 1933 *Phys. Rev. A* **43** 491
- [2] Walters H R J 2010 *Science* **330** 762
- [3] Charlton M and Humberston J W 2000 Cambridge monographs on atomic, molecular and chemical physics *Positron Physics* (Cambridge University Press)
- [4] McEachran R P and Stauffer A 2006 Positron collisions *Springer Handbook of Atomic, Molecular and Optical Physics* ed G W F Drake (Springer) p 731
- [5] Laricchia G, Armitage S, Kövér A and Murtagh D J 2008 *Adv. At. Mol. Opt. Phys.* **56** 1
- [6] Loreti A, Kadokura R, Fayer S E, Kövér A and Laricchia G 2016 *Phys. Rev. Lett.* **117** 253401
- [7] Kadyrov A S and Bray I 2002 *Phys. Rev. A* **66** 012710
- [8] Utamuratov R, Kadyrov A S, Fursa D V, Bray I and Stelbovics A T 2010 *J. Phys. B: At. Mol. Opt. Phys.* **43** 125203

- [9] Gribakin G F, Young J A and Surko C M 2010 *Rev. Mod. Phys.* **82** 2557
- [10] Ho Y K and Yan Z-C 2004 *Phys. Rev. A* **70** 032716
- [11] Umair M and Jonsell S 2016 *Phys. Rev. A* **93** 052707
- [12] Danielson J R, Ghosh S and Surko C M 2021 *J. Phys. B: At. Mol. Opt. Phys.* **54** 225201
- [13] Pietrow M, Zaleski R, Wagner A, Słomski P, Hirschmann E, Krause-Rehberg R, Liedke M O, Butterling M and Weinberger D 2021 *Phys. Chem. Chem. Phys.* **23** 11264
- [14] Naginey T C, Pollock B B, Stacy E W, Walters H R J and Whelan C T 2014 *Phys. Rev. A* **89** 012708
- [15] Pandey M K, Lin Y-C and Ho Y K 2016 *J. Phys. B: At. Mol. Opt. Phys.* **49** 034007
- [16] Donnan P H and Robicheaux F 2012 *New J. Phys.* **14** 035018
- [17] Rayment M H, Gurung L, Sheldon R E, Hogan S D and Cassidy D B 2019 *Phys. Rev. A* **100** 013410
- [18] Liu S, Ye D and Liu J 2020 *Phys. Rev. A* **101** 052704
- [19] Reeth P V, Woods D, Ward S J and Humberston J W 2016 *J. Phys. B: At. Mol. Opt. Phys.* **49** 114001
- [20] Kernoghan A A, Robinson D J R, McAlinden M T and Walters H R J 1996 *J. Phys. B: At. Mol. Opt. Phys.* **29** 2089
- [21] Zhou Y, Ratnavelu K and McCarthy I E 2005 *Phys. Rev. A* **71** 042703
- [22] Igarashi A, Toshima N and Shirai T 1996 *Phys. Rev. A* **54** 5004
- [23] Kadyrov A S and Bray I 2016 *J. Phys. B: At. Mol. Opt. Phys.* **49** 222002
- [24] Igarashi A and Toshima N 1993 *Phys. Rev. A* **47** 2386
- [25] Ghoshal A and Mandal P 2005 *Phys. Rev. A* **72** 032714
- [26] Jiao L, Wang Y and Zhou Y 2011 *Phys. Rev. A* **84** 052711
- [27] Bhatia A K 2018 *Atoms* **6** 27
- [28] Colgan J and Pindzola M S 2012 *Eur. Phys. J. D* **66** 284
- [29] Plante D R and Pindzola M S 1998 *Phys. Rev. A* **57** 1038
- [30] Yamanaka N and Kino Y 2001 *Phys. Rev. A* **64** 042715
- [31] Yamanaka N, Kino Y, Takano Y, Kudo H and Ichimura A 2003 *Phys. Rev. A* **67** 052712
- [32] Naginey T C, Stacy E W, Pollock B B, Walters H R J and Whelan C T 2014 *Phys. Rev. A* **89** 062704
- [33] Liu S, Ye D and Liu J 2020 *J. Phys. B: At. Mol. Opt. Phys.* **53** 145005
- [34] Bray I, Bray A W, Fursa D V and Kadyrov A S 2018 *Phys. Rev. Lett.* **121** 203401
- [35] Gharibnejad H, Schneider B I, Leadingham M and Schmale H J 2020 *Comput. Phys. Commun.* **252** 106808
- [36] Hu S X 2013 *Phys. Rev. Lett.* **111** 123003
- [37] Liu A and Thumm U 2014 *Phys. Rev. A* **89** 063423
- [38] Zhao X, Zhang G, Bai T, Wang J and Yu W-W 2021 *Chin. Phys. B* **30** 073201
- [39] Larkin J M, Eberly J H, Lappas D G and Grobe R 1998 *Phys. Rev. A* **57** 2572
- [40] Lappas D G, Grobe R and Eberly J H 1996 *Phys. Rev. A* **54** 3042
- [41] Kull H-J and Tikhonchuk V T 2005 *Phys. Plasmas* **12** 063301
- [42] Bauch S and Bonitz M 2009 *Contrib. Plasma Phys.* **49** 558
- [43] Kull H-J 2012 *New J. Phys.* **14** 055013
- [44] Kornev A S and Zon B A 2019 *J. Phys. B: At. Mol. Opt. Phys.* **52** 075205
- [45] Niederhausen T and Thumm U 2006 *Phys. Rev. A* **73** 041404(R)
- [46] Wang N, Jiao L G and Liu A 2019 *Chin. Phys. B* **28** 093402
- [47] Jensen S V B and Madsen L B 2020 *J. Phys. B: At. Mol. Opt. Phys.* **53** 195602
- [48] Niederhausen T, Feuerstein B and Thumm U 2004 *Phys. Rev. A* **70** 023408
- [49] Liu C L, He B, Zou S Y and Wang J G 2016 *J. Phys. B: At. Mol. Opt. Phys.* **49** 195201
- [50] Wang Z, Najjari B, Zhang S F, Ma X and Voitkiv A B 2019 *Phys. Rev. A* **100** 052710
- [51] Höhr C, Dorn A, Najjari B, Fischer D, Schröter C D and Ullrich J 2005 *Phys. Rev. Lett.* **94** 153201
- [52] deHarak B A, Nosarzewski B, Siavashpouri M and Martin N L S 2014 *Phys. Rev. A* **90** 032709
- [53] Ajana I, Nehari D, Khalil D, Taoutioui A, Agueny H and Makhoute A 2021 *Atoms* **9** 67
- [54] Ehlötzky F, Jaroń A and Kamiński J 1998 *Phys. Rep.* **297** 63
- [55] Li S-M, Zhou Z-F, Zhou J-G and Liu Y-Y 1993 *Phys. Rev. A* **47** 4960
- [56] Zheng M-Y, Qin G and Li S-M 2010 *Phys. Rev. A* **82** 033425
- [57] Joachain C J, Kylstra N J and Potvliege R M 2012 *Atoms in Intense Laser Fields* (Cambridge University Press)
- [58] He F, Becker A and Thumm U 2008 *Phys. Rev. Lett.* **101** 213002
- [59] Su Q and Eberly J H 1991 *Phys. Rev. A* **44** 5997
- [60] Feit M D, Fleck J A and Steiger A 1982 *J. Comput. Phys.* **47** 412
- [61] Krause J L, Schafer K J and Kulander K C 1992 *Phys. Rev. A* **45** 4998
- [62] Meschede D 2004 *Optics, Light and Lasers* (WILEY-VCH Verlag)
- [63] We observe sloping interference fringes at extremely low incident energies, e.g.,  $E_0 = 0.01$
- [64] At  $k = 0$ , the scattering amplitudes in post form in the target excitation and Ps formation channels are roughly proportional to  $\langle \psi_n | V(x_2) | \psi_1 \rangle$  and  $\langle \phi_n | V(x_2) | \psi_1 \rangle$ , respectively. Considering both, the soft-Coulomb potential and the initial state have even parity, the final states must also have even parity. In practical simulations, however, the odd-parity states are not strictly forbidden, due to the dynamical scattering process.
- [65] Lucas H, Zimmermann M, Betelu, S I, Schleich W P and Efremov M A 2019 *Phys. Rev. A* **100** 012709
- [66] Liu Y, Yu Y-C and Chen S 2021 *Phys. Rev. A* **104** 033303
- [67] Nishida Y 2018 *Phys. Rev. A* **97** 061603
- [68] Guijarro G, Pricoupenko A, Astrakharchik G E, Boronat J and Petrov D S 2018 *Phys. Rev. A* **97** 061605
- [69] Aronson I, Kleinman C J and Spruch L 1971 *Phys. Rev. A* **4** 841
- [70] Mitroy J, Bromley M W J and Ryzhikh G G 2002 *J. Phys. B: At. Mol. Opt. Phys.* **35** R81
- [71] Armour E A G 1978 *J. Phys. B: At. Mol. Opt. Phys.* **11** 2803
- [72] Lehtovaara L, Toivanen J and Eloranta J 2007 *J. Comput. Phys.* **221** 148
- [73] Grobe R and Eberly J H 1993 *Phys. Rev. A* **48** 4664